

# Surface Integral Method for the Second Harmonic Generation in Metal Nanoparticles

Carlo Forestiere,<sup>1,2</sup> Antonio Capretti,<sup>1</sup> and Giovanni Miano<sup>1,\*</sup>

<sup>1</sup>*Department of Electrical Engineering and Information Technology,  
Università degli Studi di Napoli Federico II, via Claudio 21, Napoli, 80125, Italy*

<sup>2</sup>*Department of Electrical and Computer Engineering & Photonics Center,  
Boston University, 8 Saint Marys Street, Boston, Massachusetts*

Second harmonic (SH) radiation in metal nanoparticles is generated by both nonlocal-bulk and local-surface SH sources, induced by the electromagnetic field at the fundamental frequency. We propose a surface integral equation (SIE) method for evaluating the SH radiation generated by metal nanoparticles with arbitrary shapes, considering all SH sources. We demonstrate that the contribution of the nonlocal-bulk SH sources to the SH electromagnetic field can be taken into account through equivalent surface electric and magnetic currents. We numerically solve the SIE problem by using the Galerkin method and the Rao-Wilton-Glisson basis functions in the framework of the distribution theory. The accuracy of the proposed method is verified by comparison with the SH-Mie analytical solution. As an example of a complex-shaped particle, we investigate the SH scattering by a triangular nano-prism. This method paves the way for a better understanding of the SH generation process in arbitrarily shaped nanoparticles and can also have a high impact in the design of novel nanoplasmonic devices with enhanced SH emission.

## I. INTRODUCTION

The study of nonlinear optical properties of noble metal nanoparticles (NPs) has become a very active research field, stimulated by both the maturity of nanofabrication techniques and the appeal of the potential applications [1]. Noble metal nanoparticles support localized surface plasmon (LSP) resonances, consisting in the collective oscillations of the conduction electrons [2]. LSPs can significantly enhance both the linear and nonlinear scattering [3], enabling strong nonlinear optical effects at relatively low excitation powers.

The second harmonic (SH) generation is a nonlinear optical process in which two photons of the same frequency, *i.e.* the fundamental frequency, interact with the material and generate one photon of twice the frequency. SH generation from noble metal NPs takes place in the bulk of the particle and on its surface. In particular, the electromagnetic field at the fundamental frequency induces nonlocal-bulk and local-surface SH sources, whereas the local-bulk SH sources are absent due to the centrosymmetry of the material [4]. The local-surface SH sources are due to the symmetry breaking at the interface between the NP and the embedding medium [5]. The relative weights of the different nonlinear sources depend on the NP shape and size, and on the optical properties of the metal at both the fundamental and the SH frequencies [6].

Several analytical models have been developed to describe the SH scattering from centrosymmetric NPs of simple shapes such as spheres and cylinders. In particular, Dadap *et. al* [5] studied the SH radiation generated from the local-surface SH sources in a sphere with radius much smaller than the wavelength of the exciting

light (Rayleigh limit). This model was later extended in [7, 8], considering also the nonlocal-bulk sources. A full-wave theory of the SH generation by a sphere of centrosymmetric material featuring SH local-surface sources has been proposed in [9]. This approach has been recently extended to model aggregates of spheres [10] but, also in this case, only the local-surface SH sources have been taken into account. A full-wave analytical theory has been also proposed for the SH scattering of light by a cylinder of infinite length [11].

The last few decades have witnessed a continuous improvement of nanofabrication techniques and a large variety of complex shapes can be controllably achieved nowadays. This fact allows for an accurate tuning of the spectral position of the LSP resonance of a NP and stimulates the demand for numerical tools to model the linear and non-linear behavior of NPs with arbitrary shapes. In fact, De Beer *et al.* [12] presented a theoretical framework for solving the SH generation problem for particles of arbitrary shape in the low contrast limit. Makitalo *et. al.* [13] introduced a surface integral equation (SIE) formulation for studying the nonlinear scattering from arbitrarily shaped particles taking into account only the local-surface SH sources. Benedetti *et. al.* [14] developed a volume integral equation (VIE) formulation based on the dyadic Green function for the study of non-linear scattering properties of arbitrarily shaped particles due to both nonlocal-bulk and local-surface contributions. However, unlike SIE formulations, the VIE formulations require the discretization of the entire NP volume, resulting in an higher memory occupancy and longer computational time.

In this paper, we present a SIE formulation of the SH generation problem for three dimensional, arbitrarily shaped nanoparticles made of centrosymmetric and lossy materials, including both the nonlocal-bulk and local-surface nonlinear polarization sources. The nonlocal-bulk polarization sources play an important role and has

---

\* Corresponding author: miano@unina.it

to be considered in any realistic model of SH generation [14, 15]. The problem is treated in the frequency domain under the undepleted-pump approximation. In particular, we demonstrate that the contribution of the nonlocal-bulk sources to the SH electromagnetic field can be taken into account by introducing fictitious electric and magnetic currents on the particle boundary, leading to a great simplification of the numerical problem. The excitation vectors of the SIE system have been derived in the framework of the distribution theory in order to correctly account for the discontinuity of the discrete representation of the SH sources.

The paper is organized as follows. Section 2 presents the mathematical statement of the problem along with the expression of both the nonlocal-bulk and the local-surface nonlinear polarization sources of the SH radiation. Then Section 3 is devoted to the SIE formulation and its numerical solution through the Galerkin method. Section 4 deals with the validation of the method, accomplished through an extensive comparison with the full wave SH Mie solution for nanoparticles with spherical shapes proposed in ref. [16]. Finally, the SH scattering from a gold triangular prism is presented.

## II. STATEMENT OF THE PROBLEM

In this section, we formulate the problem of SH generation from a lossy NP of arbitrary shape in a homogeneous medium, when it is illuminated by a time-harmonic electromagnetic field at frequency  $\omega$ . The domain of the electromagnetic field is the entire space  $\mathbb{R}^3$ , which is divided into the interior of the metal domain  $\overset{\circ}{V}_i$ , the external medium  $\overset{\circ}{V}_e$  and the interface  $S$ . The closed surface  $S$  is oriented such that its normal  $\mathbf{n}$  points outward. Furthermore,  $\mathbf{r}$  denotes the position vector with respect to an arbitrary reference point  $O$ . Since the intensities of the SH fields generated by noble metals NP are always order of magnitude weaker than the intensities of the pump fields, we can assume that the SH fields do not couple back to the fundamental fields (*undepleted-pump approximation*). Therefore, the non-linear electromagnetic problem can be decomposed in two linear scattering problems at the fundamental frequency and at the SH frequency. The nonlinear response of the material is described by the SH polarization sources induced by the fundamental electric field.

We denote with  $(\mathbf{E}_l^{(\omega)}, \mathbf{H}_l^{(\omega)})$  the fundamental fields at frequency  $\omega$  in the region  $\overset{\circ}{V}_l$  with  $l = i, e$ , and with  $(\mathbf{E}_l^{(2\omega)}, \mathbf{H}_l^{(2\omega)})$  the SH field at frequency  $2\omega$ . We use the convention  $\mathbf{a}(\mathbf{r}) = \Re \{ \mathbf{A}^{(\Omega)}(\mathbf{r}) \exp(j\Omega t) \}$  for representing a time harmonic electromagnetic field. Furthermore, we denote with  $(\mathbf{E}_0^{(\omega)}, \mathbf{H}_0^{(\omega)})$  the pump fields incident in  $\overset{\circ}{V}_e$ , with  $(\varepsilon_i \{ \Omega \}, \mu_i)$  the linear permittivity at frequency  $\Omega$  and the permeability of the metal, and with

and  $(\varepsilon_e, \mu_e)$  the permeability and the permittivity of the embedding medium. In order to calculate the SH radiation generated by the metal particle we have to evaluate: 1) the electric fields  $\mathbf{E}_l^{(\omega)}$  at the fundamental frequency induced by the pump electromagnetic field; 2) the bulk and surface nonlinear sources generated by  $\mathbf{E}_l^{(\omega)}$  and 3) the SH fields  $(\mathbf{E}_l^{(2\omega)}, \mathbf{H}_l^{(2\omega)})$  generated by the nonlinear sources.

Aiming at the solution of scattering problem at the fundamental frequency, we introduce the scattered fields  $(\mathbf{E}_l^{(\omega,s)}, \mathbf{H}_l^{(\omega,s)})$  with  $l = i, e$ , defined as:

$$\begin{cases} \mathbf{E}_e^{(\omega,s)} = \mathbf{E}_e^{(\omega)} - \mathbf{E}_0^{(\omega)} \\ \mathbf{H}_e^{(\omega,s)} = \mathbf{H}_e^{(\omega)} - \mathbf{H}_0^{(\omega)} \end{cases} \text{ in } \overset{\circ}{V}_e \quad \begin{cases} \mathbf{E}_i^{(\omega,s)} = \mathbf{E}_i^{(\omega)} \\ \mathbf{H}_i^{(\omega,s)} = \mathbf{H}_i^{(\omega)} \end{cases} \text{ in } \overset{\circ}{V}_i$$

The scattered fields at the fundamental frequency can be determined by solving the problem:

$$\begin{cases} \nabla \times \mathbf{E}_l^{(\omega,s)} = -j\omega\mu_l \mathbf{H}_l^{(\omega,s)} \\ \nabla \times \mathbf{H}_l^{(\omega,s)} = j\omega\varepsilon_l \{ \omega \} \mathbf{E}_l^{(\omega,s)} \end{cases} \text{ in } \overset{\circ}{V}_l, \quad \text{with } l = i, e, \\ \begin{cases} \mathbf{n} \times (\mathbf{E}_e^{(\omega,s)} - \mathbf{E}_i^{(\omega,s)}) = -\mathbf{n} \times \mathbf{E}_0^{(\omega)} \\ \mathbf{n} \times (\mathbf{H}_e^{(\omega,s)} - \mathbf{H}_i^{(\omega,s)}) = -\mathbf{n} \times \mathbf{H}_0^{(\omega)} \end{cases} \text{ on } S, \end{cases} \quad (1)$$

with the radiation condition at infinity. Once the solution of problem 1 has been obtained, the SH polarization sources can be calculated.

Noble metals are centrosymmetric materials, therefore the leading term of the bulk nonlinear polarization density  $\mathbf{P}_b^{(2\omega)}$  is:

$$\mathbf{P}_b^{(2\omega)} = \varepsilon_0 \overset{\leftrightarrow}{\chi}_b^{(2)} : \mathbf{E}_i^{(\omega)} (\nabla \mathbf{E}_i^{(\omega)}) \quad \text{for } \mathbf{r} \in \overset{\circ}{V}_i \quad (2)$$

where  $\overset{\leftrightarrow}{\chi}_b^{(2)}$  is the quadrupolar contribution to the second-order nonlinear bulk susceptibility of the metal. In the case of isotropic and homogeneous material the relation 2 becomes:

$$\mathbf{P}_b^{(2\omega)} = \varepsilon_0 \gamma \nabla (\mathbf{E}_i^{(\omega)} \cdot \mathbf{E}_i^{(\omega)}) + \varepsilon_0 \delta' (\mathbf{E}_i^{(\omega)} \cdot \nabla) \mathbf{E}_i^{(\omega)}, \quad (3)$$

where  $\gamma$  and  $\delta'$  are material parameters [26]. By using the vectorial identity  $\frac{1}{2} \nabla (\mathbf{A} \cdot \mathbf{A}) = \mathbf{A} \times (\nabla \times \mathbf{A}) + (\mathbf{A} \cdot \nabla) \mathbf{A}$  together with the Maxwell equations, we have:

$$\mathbf{P}_b^{(2\omega)} = \mathbf{P}_{\gamma'}^{(2\omega)} + \mathbf{P}_{\delta'}^{(2\omega)} \quad (4)$$

where  $\mathbf{P}_{\gamma'}^{(2\omega)} = \varepsilon_0 \gamma' \nabla (\mathbf{E}_i^{(\omega)} \cdot \mathbf{E}_i^{(\omega)})$ ,  $\mathbf{P}_{\delta'}^{(2\omega)} = \delta' j\omega/c^2 \mathbf{E}_i^{(\omega)} \times \mathbf{H}_i^{(\omega)}$ , and  $\gamma' = \gamma + \frac{\delta'}{2}$ . Although eqs. 3 and 4 are mathematically equivalent, the latter is easier to treat numerically.

The local-surface SH polarization sources  $\mathbf{P}_S^{(2\omega)}$  are:

$$\mathbf{P}_S^{(2\omega)} = \varepsilon_0 \overset{\leftrightarrow}{\chi}_S^{(2)} : \mathbf{E}_i^{(\omega)} \mathbf{E}_i^{(\omega)}, \quad (5)$$

where  $\overset{\leftrightarrow}{\chi}_S^{(2)}$  is the second-order surface nonlinear susceptibility. Since the NP surface has an isotropic symmetry with a mirror plane perpendicular to it, the surface-susceptibility tensor  $\overset{\leftrightarrow}{\chi}_S^{(2)}$  has only three non-vanishing and independent elements,  $\chi_{\perp\perp\perp}^{(2)}$ ,  $\chi_{\perp\parallel\parallel}^{(2)}$  and  $\chi_{\parallel\perp\perp}^{(2)} = \chi_{\parallel\parallel\perp}^{(2)}$ , where  $\perp$  and  $\parallel$  refer to the orthogonal and tangential components to the nanoparticle surface. Therefore, we have:

$$\mathbf{P}_S^{(2\omega)} = \epsilon_0 \left[ \chi_{\perp\perp\perp}^{(2)} \mathbf{nnn} + \chi_{\perp\parallel\parallel}^{(2)} (\mathbf{nt}_1\mathbf{t}_1 + \mathbf{nt}_2\mathbf{t}_2) + \chi_{\parallel\perp\perp}^{(2)} (\mathbf{t}_1\mathbf{nt}_1 + \mathbf{t}_2\mathbf{nt}_2) \right] : \mathbf{E}_i^{(\omega)} \mathbf{E}_i^{(\omega)}, \quad (6)$$

where  $(\mathbf{t}_1, \mathbf{t}_2, \mathbf{n})$  is a system of three orthonormal vectors locally defined on the particle surface. The contribution of tangential and normal component of the surface nonlinear polarization are taken into account by introducing the surface electric  $\boldsymbol{\pi}_S^{(e)}$  and magnetic  $\boldsymbol{\pi}_S^{(m)}$  current densities [4]:

$$\boldsymbol{\pi}_S^{(e)} = j2\omega \mathbf{P}_t^S, \quad (7a)$$

$$\boldsymbol{\pi}_S^{(m)} = \frac{1}{\epsilon_0} \mathbf{n} \times \nabla_S P_n^S, \quad (7b)$$

where  $\mathbf{P}_t^S = -\mathbf{n} \times \mathbf{n} \times \mathbf{P}_S^{(2\omega)}$  and  $P_n^S = \mathbf{P}_S^{(2\omega)} \cdot \mathbf{n}$ .

We determine the SH fields by solving non-homogeneous problem:

$$\begin{cases} \nabla \times \mathbf{E}_e^{(2\omega)} = -j2\omega\mu_e \mathbf{H}_e^{(2\omega)} \\ \nabla \times \mathbf{H}_e^{(2\omega)} = j2\omega\epsilon_e \mathbf{E}_e^{(2\omega)} \end{cases} \text{ in } \overset{\circ}{V}_e, \quad (8a)$$

$$\begin{cases} \nabla \times \mathbf{E}_i^{(2\omega)} = -j2\omega\mu_i \mathbf{H}_i^{(2\omega)} \\ \nabla \times \mathbf{H}_i^{(2\omega)} = j2\omega\epsilon_i \{2\omega\} \mathbf{E}_i^{(2\omega)} + j2\omega (\mathbf{P}_{\gamma'} + \mathbf{P}_{\delta'}) \end{cases} \text{ in } \overset{\circ}{V}_i, \quad (8b)$$

$$\begin{cases} \mathbf{n} \times (\mathbf{E}_e^{(2\omega)} - \mathbf{E}_i^{(2\omega)}) = -\boldsymbol{\pi}_S^{(m)} \\ \mathbf{n} \times (\mathbf{H}_e^{(2\omega)} - \mathbf{H}_i^{(2\omega)}) = \boldsymbol{\pi}_S^{(e)} \end{cases} \text{ on } S, \quad (8c)$$

with the radiation condition at infinity. Due to the linearity of the problem 8a-8c, its general solution is the sum of the solution of the homogeneous equation and one particular solution of the inhomogeneous equation. The eq. 8b is satisfied by the particular solution:

$$\begin{cases} \mathbf{E}_{part} = \mathbf{E}_{\gamma'}^{(2\omega)} + \mathbf{E}_{\delta'}^{(2\omega)} \\ \mathbf{H}_{part} = \mathbf{H}_{\delta'}^{(2\omega)}, \end{cases} \quad (9)$$

where:

$$\mathbf{E}_{\gamma'}^{(2\omega)} = -\frac{\epsilon_0 \gamma'}{\epsilon_i \{2\omega\}} \nabla \left( \mathbf{E}_i^{(\omega)} \cdot \mathbf{E}_i^{(\omega)} \right), \quad (10)$$

$$\begin{aligned} \mathbf{E}_{\delta'}^{(2\omega)} = & -j\omega\mu_0 \iiint_{V_i} \mathbf{J}_{\delta'}(\mathbf{r}') g_i^{(2\omega)}(\mathbf{r} - \mathbf{r}') dV' \\ & - \frac{1}{\epsilon_i \{2\omega\}} \nabla \left[ \iiint_{V_i} \rho_{\delta'}(\mathbf{r}') g_i^{(2\omega)}(\mathbf{r} - \mathbf{r}') dV' \right. \\ & \left. + \iint_S \eta_{\delta'}(\mathbf{r}') g_i^{(2\omega)}(\mathbf{r} - \mathbf{r}') dS' \right], \quad (11) \end{aligned}$$

$$\mathbf{H}_{\delta'}^{(2\omega)} = \nabla \times \iiint_{V_i} \mathbf{J}_{\delta'}(\mathbf{r}') g_i^{(2\omega)}(\mathbf{r} - \mathbf{r}') dV'. \quad (12)$$

The volumetric current density  $\mathbf{J}_{\delta'}$ , the volumetric charge density  $\rho_{\delta'}$  and the surface charge density  $\eta_{\delta'}$  are given by:

$$\begin{aligned} \mathbf{J}_{\delta'}(\mathbf{r}') &= j2\omega \mathbf{P}_{\delta'}, \\ \rho_{\delta'}(\mathbf{r}') &= -\nabla \cdot \mathbf{P}_{\delta'}, \\ \eta_{\delta'}(\mathbf{r}') &= \mathbf{n} \cdot \mathbf{P}_{\delta'}, \end{aligned} \quad (13)$$

where the quantity  $\mathbf{P}_{\delta'}$  has been defined in eq. 4 and  $g_i^{(\Omega)}$  is the homogeneous space Green's function in the internal medium, *i.e.*  $g_i^{(2\omega)}(\mathbf{r} - \mathbf{r}') = \frac{e^{-jk_i \{2\omega\} |\mathbf{r} - \mathbf{r}'|}}{4\pi |\mathbf{r} - \mathbf{r}'|}$ ,  $k_i \{2\omega\} = 2\omega \sqrt{\mu_i \epsilon_i \{2\omega\}}$ . Therefore, the solution of the non-homogeneous problem defined by eqs. 8a-8c can be written as:

$$\begin{cases} \mathbf{E}_i^{(2\omega)} = \tilde{\mathbf{E}}_i^{(2\omega)} + \mathbf{E}_{\gamma'}^{(2\omega)} + \mathbf{E}_{\delta'}^{(2\omega)} \\ \mathbf{H}_i^{(2\omega)} = \tilde{\mathbf{H}}_i^{(2\omega)} + \mathbf{H}_{\delta'}^{(2\omega)} \end{cases} \quad \begin{cases} \mathbf{E}_e^{(2\omega)} = \tilde{\mathbf{E}}_e^{(2\omega)} \\ \mathbf{H}_e^{(2\omega)} = \tilde{\mathbf{H}}_e^{(2\omega)} \end{cases} \quad (14)$$

where  $(\tilde{\mathbf{E}}_l^{(2\omega)}, \tilde{\mathbf{H}}_l^{(2\omega)})$  with  $l = i, e$  is the solution of the problem:

$$\begin{cases} \nabla \times \tilde{\mathbf{E}}_l^{(2\omega)} = -j2\omega\mu_l \tilde{\mathbf{H}}_l^{(2\omega)} \\ \nabla \times \tilde{\mathbf{H}}_l^{(2\omega)} = j2\omega\epsilon_l \{2\omega\} \tilde{\mathbf{E}}_l^{(2\omega)} \end{cases} \text{ in } \overset{\circ}{V}_l \quad \text{with } l = i, e, \quad (15)$$

$$\begin{cases} \mathbf{n} \times (\tilde{\mathbf{E}}_e^{(2\omega)} - \tilde{\mathbf{E}}_i^{(2\omega)}) = -\boldsymbol{\pi}_S^{(m)} - \boldsymbol{\pi}_{\gamma'}^{(m)} - \boldsymbol{\pi}_{\delta'}^{(m)} \\ \mathbf{n} \times (\tilde{\mathbf{H}}_e^{(2\omega)} - \tilde{\mathbf{H}}_i^{(2\omega)}) = \boldsymbol{\pi}_S^{(e)} + \boldsymbol{\pi}_{\delta'}^{(e)} \end{cases} \text{ on } S, \quad (16)$$

with the radiation condition at infinity, where:

$$\begin{aligned} \boldsymbol{\pi}_{\gamma'}^{(m)} &= \frac{1}{\epsilon_0} \mathbf{n} \times \nabla_S P_n^{\gamma'}, \\ \boldsymbol{\pi}_{\delta'}^{(m)} &= -\mathbf{n} \times \mathbf{E}_{\delta'}^{(2\omega)} \\ \boldsymbol{\pi}_{\delta'}^{(e)} &= \mathbf{n} \times \mathbf{H}_{\delta'}^{(2\omega)} \end{aligned} \quad (17)$$

and

$$P_n^{\gamma'} = \frac{\epsilon_0^2 \gamma'}{\epsilon_i \{2\omega\}} \left( \mathbf{E}_i^{(\omega)} \cdot \mathbf{E}_i^{(\omega)} \right). \quad (18)$$

In conclusion, both nonlocal-bulk sources can be equivalently treated by using superficial electric and magnetic currents. In particular, the source arising from  $\gamma'$  can

be associated to a fictitious surface polarization  $P_n^{\gamma'} \mathbf{n}$ , as already shown in [27]. Unlike ref. [27], this approach has also the advantage of the determination of the electromagnetic field due to the nonlocal-bulk sources  $\mathbf{P}_{\gamma'}^{(2\omega)}$  both outside and inside the particle.

### III. SURFACE INTEGRAL EQUATIONS

Let us define, for the same geometry described in the previous section, an auxiliary scattering problem that includes both the fundamental and the SH problems as special cases. Let  $\boldsymbol{\pi}_0^{(\Omega,e)}$ ,  $\boldsymbol{\pi}_0^{(\Omega,m)}$  be the impressed electric and magnetic sources on  $S$ . We denote with  $(\mathbf{E}_l^{(\Omega,s)}, \mathbf{H}_l^{(\Omega,s)})$   $l = i, e$  the fields solution of the problem:

$$\begin{cases} \nabla \times \mathbf{E}_l^{(\Omega,s)} = -j\Omega\mu_l \mathbf{H}_l^{(\Omega,s)} \\ \nabla \times \mathbf{H}_l^{(\Omega,s)} = j\Omega\varepsilon_l \{\Omega\} \mathbf{E}_l^{(\Omega,s)} \end{cases} \quad \text{in } \overset{\circ}{V}_l \quad \text{with } l = i, e, \\ \begin{cases} \mathbf{n} \times (\mathbf{E}_e^{(\Omega,s)} - \mathbf{E}_i^{(\Omega,s)}) = -\boldsymbol{\pi}_0^{(\Omega,m)} \\ \mathbf{n} \times (\mathbf{H}_e^{(\Omega,s)} - \mathbf{H}_i^{(\Omega,s)}) = +\boldsymbol{\pi}_0^{(\Omega,e)} \end{cases} \quad \text{on } S, \end{cases} \quad (19)$$

with the radiation condition at infinity. We obtain the fundamental problem described of eq. 1, by substituting  $\Omega = \omega$  and

$$\begin{cases} \boldsymbol{\pi}_0^{(\omega,e)} = -\mathbf{n} \times \mathbf{H}_0^{(\omega)} \\ \boldsymbol{\pi}_0^{(\omega,m)} = \mathbf{n} \times \mathbf{E}_0^{(\omega)}. \end{cases} \quad (20)$$

Analogously, we can obtain the SH problem described by eq. 16 by substituting  $\Omega = 2\omega$  and

$$\begin{cases} \boldsymbol{\pi}_0^{(2\omega,e)} = \boldsymbol{\pi}_S^{(e)} + \boldsymbol{\pi}_{\delta'}^{(e)} \\ \boldsymbol{\pi}_0^{(2\omega,m)} = \boldsymbol{\pi}_S^{(m)} + \boldsymbol{\pi}_{\delta'}^{(m)} + \boldsymbol{\pi}_{\gamma'}^{(m)}. \end{cases} \quad (21)$$

We now derive the surface integral formulation for the problem of eq. 19. By invoking the Love's equivalent principle [28] for the exterior medium, the region  $\overset{\circ}{V}_i$  is filled up with the same material of the region  $\overset{\circ}{V}_e$ , and the sources are removed. The equivalent currents  $(\mathbf{j}_e^{(\Omega,e)}, \mathbf{j}_e^{(\Omega,m)})$ , positioned on the external page  $S_e$  of the surface  $S$ , produce the field  $(\mathbf{E}_e^{(\Omega,s)}, \mathbf{H}_e^{(\Omega,s)})$  in the region  $\overset{\circ}{V}_e$ , and null fields in the region  $\overset{\circ}{V}_i$ , *i.e.*:

$$\begin{aligned} \mathcal{E}_e^{(\Omega)} \{ \mathbf{j}_e^{(\Omega,e)}, \mathbf{j}_e^{(\Omega,m)} \} (\mathbf{r}) &= \begin{cases} \mathbf{0} & \text{if } \mathbf{r} \in \overset{\circ}{V}_i, \\ \mathbf{E}_e^{(\Omega,s)}(\mathbf{r}) & \text{if } \mathbf{r} \in \overset{\circ}{V}_e, \end{cases} \\ \mathcal{H}_e^{(\Omega)} \{ \mathbf{j}_e^{(\Omega,e)}, \mathbf{j}_e^{(\Omega,m)} \} (\mathbf{r}) &= \begin{cases} \mathbf{0} & \text{if } \mathbf{r} \in \Omega_i, \\ \mathbf{H}_e^{(\Omega,s)}(\mathbf{r}) & \text{if } \mathbf{r} \in \overset{\circ}{V}_e, \end{cases} \end{aligned} \quad (22)$$

where the sources  $(\mathbf{j}_e^{(\Omega,e)}, \mathbf{j}_e^{(\Omega,m)})$  are given by:

$$\begin{cases} \mathbf{j}_e^{(\Omega,e)} = +\mathbf{n} \times \mathbf{H}_e^{(\Omega,s)} \Big|_{S_e} \\ \mathbf{j}_e^{(\Omega,m)} = -\mathbf{n} \times \mathbf{E}_e^{(\Omega,s)} \Big|_{S_e} \end{cases} \quad (23)$$

An equivalent problem may be set up also for the region  $\overset{\circ}{V}_i$ . In this case the region  $\overset{\circ}{V}_i$  is filled up with the material with electromagnetic parameters  $(\varepsilon_i \{\Omega\}, \mu_i)$ . The equivalent currents  $(\mathbf{j}_i^{(\Omega,e)}, \mathbf{j}_i^{(\Omega,m)})$ , defined on the internal side  $S_i$  of the surface  $S$ , produce the original fields in the region  $\overset{\circ}{V}_i$  and null field in the region  $\overset{\circ}{V}_e$ , *i.e.*

$$\begin{aligned} \mathcal{E}_i^{(\Omega)} \{ \mathbf{j}_i^{(\Omega,e)}, \mathbf{j}_i^{(\Omega,m)} \} (\mathbf{r}) &= \begin{cases} \mathbf{E}_i^{(\Omega,s)}(\mathbf{r}) & \text{if } \mathbf{r} \in \overset{\circ}{V}_i \\ \mathbf{0} & \text{if } \mathbf{r} \in \overset{\circ}{V}_e \end{cases} \\ \mathcal{H}_i^{(\Omega)} \{ \mathbf{j}_i^{(\Omega,e)}, \mathbf{j}_i^{(\Omega,m)} \} (\mathbf{r}) &= \begin{cases} \mathbf{H}_i^{(\Omega,s)}(\mathbf{r}) & \text{if } \mathbf{r} \in \overset{\circ}{V}_i \\ \mathbf{0} & \text{if } \mathbf{r} \in \overset{\circ}{V}_e \end{cases} \end{aligned} \quad (24)$$

where the sources  $(\mathbf{j}_i^{(\Omega,e)}, \mathbf{j}_i^{(\Omega,m)})$  are given by:

$$\begin{cases} \mathbf{j}_i^{(\Omega,e)} = -\mathbf{n} \times \mathbf{H}_i^{(\Omega,s)} \Big|_{S_i} \\ \mathbf{j}_i^{(\Omega,m)} = +\mathbf{n} \times \mathbf{E}_i^{(\Omega,s)} \Big|_{S_i} \end{cases} \quad (25)$$

Furthermore, the sets of equivalent currents  $(\mathbf{j}_e^{(\Omega,e)}, \mathbf{j}_e^{(\Omega,m)})$  and  $(\mathbf{j}_i^{(\Omega,e)}, \mathbf{j}_i^{(\Omega,m)})$  are not independent. In fact, combining the boundary conditions of the problem 19 and the definitions 23 and 25 we obtain:

$$\begin{cases} \mathbf{j}_i^{(\Omega,e)} + \mathbf{j}_e^{(\Omega,e)} = \boldsymbol{\pi}_0^{(\Omega,e)} \\ \mathbf{j}_i^{(\Omega,m)} + \mathbf{j}_e^{(\Omega,m)} = \boldsymbol{\pi}_0^{(\Omega,m)} \end{cases} \quad (26)$$

We now consider the limit of eqs. 22 and 24 as the point  $\mathbf{r}$  approaches the surface  $S$  from its external face  $S_e$  and internal face  $S_i$ . Projecting the resulting equations on the surface  $S$  we obtain:

$$\mathcal{E}_e^{(\Omega,t)} \{ \mathbf{j}_e^{(\Omega,e)}, \mathbf{j}_e^{(\Omega,m)} \} - \mathbf{n} \times \mathbf{j}_e^{(\Omega,m)} = \mathbf{0}, \quad (27a)$$

$$\mathcal{H}_e^{(\Omega,t)} \{ \mathbf{j}_e^{(\Omega,e)}, \mathbf{j}_e^{(\Omega,m)} \} + \mathbf{n} \times \mathbf{j}_e^{(\Omega,e)} = \mathbf{0}, \quad (27b)$$

$$\mathcal{E}_i^{(\Omega,t)} \{ \mathbf{j}_i^{(\Omega,e)}, \mathbf{j}_i^{(\Omega,m)} \} + \mathbf{n} \times \mathbf{j}_i^{(\Omega,m)} = \mathbf{0}, \quad (27c)$$

$$\mathcal{H}_i^{(\Omega,t)} \{ \mathbf{j}_i^{(\Omega,e)}, \mathbf{j}_i^{(\Omega,m)} \} - \mathbf{n} \times \mathbf{j}_i^{(\Omega,e)} = \mathbf{0}, \quad (27d)$$

where we have defined the operators:

$$\begin{aligned} \mathcal{E}_l^{(\Omega,t)} \{ \mathbf{j}^{(e)}, \mathbf{j}^{(m)} \} &= -\mathbf{n} \times \mathbf{n} \times \mathcal{E}_l^{(\Omega)} \{ \mathbf{j}^{(e)}, \mathbf{j}^{(m)} \} \Big|_{S_l} \\ \mathcal{H}_l^{(\Omega,t)} \{ \mathbf{j}^{(e)}, \mathbf{j}^{(m)} \} &= -\mathbf{n} \times \mathbf{n} \times \mathcal{H}_l^{(\Omega)} \{ \mathbf{j}^{(e)}, \mathbf{j}^{(m)} \} \Big|_{S_l} \end{aligned} \quad (28)$$

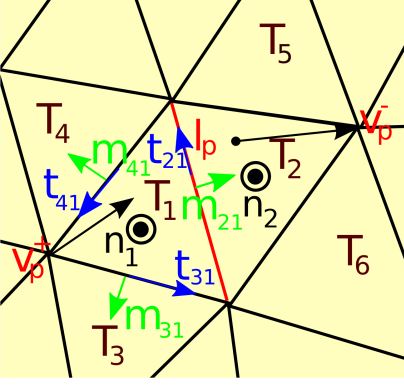


FIG. 1. The union of the two triangles  $T_1 = T_p^+, T_2 = T_p^-$  is the support of the basis function  $\mathbf{f}_p$ . For the triangle  $T_p^+ = T_1$  we show the curves  $l_{j1}$ , their tangent vectors  $\mathbf{t}_{j1}$  and binormal vectors  $\mathbf{m}_{j1}$  with  $j=2,3,4$ .

Eqs. 27a, 27c are the *T-electric field integral equations* (T-EFIE), eqs. 27d, 27b are the *T-magnetic field integral equations* (T-MFIE). By subtracting eq. 27c from eq. 27a and eq. 27d from 27b and substituting the expressions of the operators  $\mathcal{E}_l^{(\Omega)} \mathcal{H}_l^{(\Omega)}$ , provided in the appendix A, we obtain the PMCHWT formulation:

$$\mathcal{C}^{(\Omega)} \mathbf{x}^{(\Omega)} = \mathbf{y}^{(\Omega)}, \quad (29)$$

where we have defined the operator  $\mathcal{C}^{(\Omega)}$

$$\mathcal{C}^{(\Omega)} = \begin{pmatrix} \zeta_e \mathcal{T}_e^{(\Omega,t)} + \mathcal{K}_e^{(\Omega,t)} & -\zeta_i \mathcal{T}_i^{(\Omega,t)} & -\mathcal{K}_i^{(\Omega,t)} \\ -\mathcal{K}_e^{(\Omega,t)} & \zeta_e^{-1} \mathcal{T}_e^{(\Omega,t)} & +\mathcal{K}_i^{(\Omega,t)} & -\zeta_i^{-1} \mathcal{T}_i^{(\Omega,t)} \\ \mathcal{I} & 0 & \mathcal{I} & 0 \\ 0 & \mathcal{I} & 0 & \mathcal{I} \end{pmatrix},$$

the vector of unknowns  $\mathbf{x}^{(\Omega)}$ , and the excitation vector  $\mathbf{y}^{(\Omega)}$

$$\mathbf{x}^{(\Omega)} = \begin{pmatrix} \mathbf{j}_e^{(\Omega,e)} \\ \mathbf{j}_i^{(\Omega,m)} \\ \mathbf{j}_e^{(\Omega,e)} \\ \mathbf{j}_i^{(\Omega,m)} \end{pmatrix}, \quad \mathbf{y}^{(\Omega)} = \begin{pmatrix} \frac{1}{2} \mathbf{n} \times \boldsymbol{\pi}_0^{(\Omega,m)} \\ -\frac{1}{2} \mathbf{n} \times \boldsymbol{\pi}_0^{(\Omega,e)} \\ \boldsymbol{\pi}_0^{(\Omega,e)} \\ \boldsymbol{\pi}_0^{(\Omega,m)} \end{pmatrix},$$

and  $\zeta_l \{\Omega\} = \sqrt{\mu_l / \varepsilon_l \{\Omega\}}$ , with  $l = i, e$ .

#### IV. NUMERICAL SOLUTIONS

In the present section, we describe the numerical methods used to solve the PMCHWT formulation of eq. 29 both at the fundamental and at the SH frequency. In particular, we have exploited the Galerkin testing procedure to solve the SIEs, choosing the set of basis functions to coincide with the set of test functions [28].

Let us introduce a triangular mesh with  $N_t$  triangles and  $N_e$  edges. We denote with  $T_j$  the  $j^{\text{th}}$  triangle, with  $l_p$  the length of the  $p^{\text{th}}$  edge, with  $\Sigma = \cup_j T_j$  the total surface of the mesh. We denote the two triangles sharing

the  $p^{\text{th}}$  edge as  $T_1 = T_p^+$  and  $T_2 = T_p^-$  (Fig. 1). They have an area of  $A_p^+$  and  $A_p^-$  respectively. The vertices of  $T_p^+$  and  $T_p^-$ , which are opposite to the  $p^{\text{th}}$  edge, are indicated by  $v_p^+$  and  $v_p^-$  respectively. The unknown electric and magnetic currents are expanded in terms of the Rao-Wilton-Glisson (RWG) [29] functions set  $\mathbf{f}_1, \mathbf{f}_2, \dots, \mathbf{f}_{N_e}$ . The RWG function relative to the  $p^{\text{th}}$  edge is given by:

$$\mathbf{f}_p(\mathbf{r}) = \begin{cases} \mathbf{f}_p^+(\mathbf{r}) = +\frac{l_p}{2A_p^+} (\mathbf{r} - \mathbf{v}_p^+) & \mathbf{r} \in T_p^+ \\ \mathbf{f}_p^-(\mathbf{r}) = -\frac{l_p}{2A_p^-} (\mathbf{r} - \mathbf{v}_p^-) & \mathbf{r} \in T_p^- \\ \mathbf{0} & \text{otherwise} \end{cases}, \quad (30)$$

and the corresponding support is  $S_p = T_p^+ \cup T_p^-$ . We introduce also the symmetric product  $\langle \mathbf{f}, \mathbf{g} \rangle = \int_S \mathbf{f} \cdot \mathbf{g} dS$  for the space of square integrable vector functions defined on  $S$ .

We assemble the discrete operators associated to  $\mathcal{K}_l^{(\Omega,t)}$  and  $\mathcal{T}_l^{(\Omega,t)}$  by projecting on the testing function  $\mathbf{f}_p$  the image through the operators  $\mathcal{K}_l^{(\Omega,t)}$ , and  $\mathcal{T}_l^{(\Omega,t)}$  of the basis function  $\mathbf{f}_q$ . Similarly, we assemble the discrete excitation vectors for both the fundamental and SH problem by projecting on the testing function  $\mathbf{f}_p$  the fields  $\boldsymbol{\pi}_0^{(\omega,e)}$ ,  $\boldsymbol{\pi}_0^{(\omega,m)}$ ,  $\boldsymbol{\pi}_0^{(2\omega,e)}$ ,  $\boldsymbol{\pi}_0^{(2\omega,m)}$ .

In order to compute the non linear sources we need to evaluate the fundamental field on the internal side of the surface  $S$ :

$$\mathbf{E}_i^{(\omega)}(\mathbf{r}) \Big|_{S_i} = \mathbf{E}_{i,t}^{(\omega)}(\mathbf{r}) \Big|_{S_i} + E_{i,n}^{(\omega)}(\mathbf{r}) \Big|_{S_i} \mathbf{n},$$

where the tangent  $\mathbf{E}_{i,t}^{(\omega)}$  and normal component  $E_{i,n}^{(\omega)}$  of the electric field are:

$$\mathbf{E}_{i,t}^{(\omega)}(\mathbf{r}) \Big|_{S_i} = -\mathbf{n} \times \mathbf{j}_i^{(\omega,m)}(\mathbf{r}),$$

$$E_{i,n}^{(\omega)}(\mathbf{r}) \Big|_{S_i} = -j \frac{\nabla_S \cdot \mathbf{j}_i^{(\omega,e)}(\mathbf{r})}{\omega \varepsilon_i \{\omega\}}.$$

Since the equivalent electric current  $\mathbf{j}_i^{(\omega,e)}(\mathbf{r})$  is represented through the linear RWGs functions,  $E_{i,n}^{(\omega)}(\mathbf{r})$  is a piecewise *constant* function presenting a discontinuity of the first kind on the edges of the triangles. As a consequence,  $P_n^S$  (defined in eq. 6) is a piecewise constant function on the mesh and the calculation of the surface gradients  $\nabla_S P_n^S$  needed to obtain  $\boldsymbol{\pi}_m^{(2\omega)}$  (see eq. 7b) has to be carried out in the framework of the distribution theory.

We now introduce the following notations. For each triangle of the mesh, e.g.  $T_1 = T_p^+$  in Fig. 1, we define the curve  $l_{j,1}$  having as support the edge of the triangle  $T_1$  shared with the triangle  $T_j$ , which is oriented counter-clockwise when viewed from the end of the vector  $\mathbf{n}_1$ ;  $\mathbf{t}_{j,1}$  is its tangent vector, and  $\mathbf{m}_{j,1} = \mathbf{t}_{j,1} \times \mathbf{n}_1$  is its binormal vector (orthogonal to both  $\mathbf{t}_{j,1}$  and  $\mathbf{n}_1$ ) (Fig. 1). Analogous quantities are also defined for the triangle  $T_2 = T_p^-$ . Moreover, we denote with  $P_n^S \Big|_{T_j}$  the value of the function

$P_n^S$  on the triangle  $T_j$ . In order to simplify the treatment, we now assume that the triangles  $\{T_j, j = 1 \dots 6\}$  are coplanar. This hypothesis is always true for particles of regular shapes and sufficiently dense meshes. The gradient of  $P_n^S$  on the support of  $\mathbf{f}_p$  can be written in the distribution sense as:

$$\begin{aligned} \nabla_S P_n^S = & \sum_{j=2,3,4} \left( P_n^S|_{T_j} - P_n^S|_{T_1} \right) \mathbf{m}_{j1} \delta_{j1} + \\ & \sum_{j=5,6} \left( P_n^S|_{T_j} - P_n^S|_{T_2} \right) \mathbf{m}_{j2} \delta_{j2} + \end{aligned} \quad (31)$$

where the function  $\delta_{j1}$  and  $\delta_{j2}$  are Dirac functions impulsive on the edge  $l_{j1}$  and  $l_{j2}$  respectively and 0 elsewhere on  $\Sigma$ , such that  $\iint_{\Sigma} \delta_{1j} dS = 1$ ,  $\iint_{\Sigma} \delta_{2j} dS = 1$ . In the appendix B we report the explicit expressions of the discrete excitation vectors  $\langle \mathbf{f}_p, \boldsymbol{\pi}_S^{(m)} \rangle$  and  $\langle \mathbf{f}_p, \mathbf{n} \times \boldsymbol{\pi}_S^{(m)} \rangle$ .

Similarly, in order to compute the magnetic surface currents  $\boldsymbol{\pi}_{\gamma'}^{(m)}$  introduced in eq. 17, we need to calculate the gradient of  $P_n^{\gamma'}$ .  $P_n^{\gamma'}$  is a piecewise quadratic function presenting a discontinuity of the first kind along the mesh edges. Therefore, we obtain:

$$\nabla_S P_n^{\gamma'} = \begin{cases} \sum_{j=2,3,4} \left( P_n^{\gamma'}|_{T_j}(\mathbf{r}) - P_n^{\gamma'}|_{T_1}(\mathbf{r}) \right) \mathbf{m}_{j1} \delta_{j1} + \sum_{j=5,6} \left( P_n^{\gamma'}|_{T_j}(\mathbf{r}) - P_n^{\gamma'}|_{T_2}(\mathbf{r}) \right) \mathbf{m}_{j2} \delta_{j2} & \text{if } \mathbf{r} \in \partial T_1 \cup \partial T_2, \\ \nabla_S P_n^{\gamma'}|_{T_1}(\mathbf{r}) & \text{if } \mathbf{r} \in \overset{\circ}{T}_1, \\ \nabla_S P_n^{\gamma'}|_{T_2}(\mathbf{r}) & \text{if } \mathbf{r} \in \overset{\circ}{T}_2, \end{cases} \quad (32)$$

and  $P_n^{\gamma'}|_{T_j}(\mathbf{r})$  is the restriction of the function  $P_n^{\gamma'}(\mathbf{r})$  to the interior of the triangle  $T_j$ . In the appendix B we report the explicit expressions of the discrete excitation vectors  $\langle \mathbf{f}_p, \boldsymbol{\pi}_{\gamma'}^{(m)} \rangle$  and  $\langle \mathbf{f}_p, \mathbf{n} \times \boldsymbol{\pi}_{\gamma'}^{(m)} \rangle$ .

Aiming at the evaluation of the excitation terms associated to  $\mathbf{P}_{\delta'}$  we introduce a tetrahedral mesh of the particle volume  $V_i$ . Then, we calculate the quantities  $\mathbf{J}_{\delta'}$ ,  $\rho_{\delta'}$  and  $\eta_{\delta'}$  in the quadrature points of the volumetric mesh using the electric field  $\mathbf{E}_i^{(\omega)}$  and the magnetic field  $\mathbf{H}_i^{(\omega)}$  inside the particle at the fundamental frequency.  $\mathbf{E}_i^{(\omega)}$  and  $\mathbf{H}_i^{(\omega)}$  are calculated using eq. A2 in combination with the methods described in [30]. The derivation of the discrete excitation vectors is straightforward in the Galerkin formalism, and their expressions are reported in the appendix B.

## V. DISCUSSION

In the first part of this section, we validate our formulation for the problem of the SH generation from an isolated gold sphere using the full wave SH Mie solution (SH-Mie) of the problems 1 and 16. The SH-Mie solution has been obtained by expanding the pump field, the non-linear sources and the SH fields in series of vector spherical wave functions [16]. Then, we investigate the SH generation properties of a triangular nano-prism. The scatterers are homogeneous gold particles, embedded in air. The investigated physical quantity is the SH radiated

power per unit solid angle collected along the direction  $\mathbf{k}$

$$dP^{(\Omega)}/d\Omega(\mathbf{k}) = \lim_{\|\mathbf{r}\| \rightarrow +\infty} \left[ \frac{r^2}{2\zeta_e\{\Omega\}} \left\| \mathbf{E}_e^{(\Omega)}(\mathbf{k}) \right\|^2 \right]. \quad (33)$$

The gold dispersion is modeled by fitting experimental data [31]. The integrals involved in the numerical solution have been evaluated using four Gauss quadrature points for each triangle, and their singularities have been managed exploiting singularity extraction techniques [30]. The volume integrals have been evaluated using a single Gauss quadrature point for each tetrahedron.

The gold sphere is excited by a plane wave of unitary intensity, namely  $\mathbf{E}_0^{(\omega)} = \exp(-j\omega\sqrt{\varepsilon_e\mu_e}z) \hat{\mathbf{x}}$  propagating along the positive direction of the  $z$ -axis and linearly polarized along  $x$ . The exciting wavelength corresponds to the plasmonic resonance of a gold spherical particle in the Rayleigh limit, *i.e.* 520nm. The relative permittivity used in the calculations are  $\varepsilon_i(520nm) = -3.88 - 2.63j$  and  $\varepsilon_i(260nm) = -1.20 - 4.67j$  for the fundamental and the SH problem, respectively. From both theoretical and experimental studies it results that the component  $\chi_{\perp\parallel\parallel}^{(2)}$  only weakly contributes to the SH generation from noble metals [32]. Moreover, in the case of the sphere following Bachelier et al. [32] we also neglect the contribution of the  $\delta'$  source. Following [32, 33] we express the parameters  $\chi_{\perp\perp\perp}$ ,  $\chi_{\parallel\perp\parallel}$ , and  $\gamma$  through the dimensionless *Rudnick-Stern parameters*  $a$ ,  $b$  and  $d$  [33] as follows:

$$\left[ \chi_{\perp\perp\perp}^{(2)}, \chi_{\parallel\perp\parallel}^{(2)}, \gamma \right] = - \left[ \frac{a}{4}, \frac{b}{2}, \frac{d}{8} \right] \chi_b^{(1)}(\omega) \frac{\omega_p^2 \varepsilon_0}{\omega^2 \varepsilon n_0}, \quad (34)$$

where  $\chi_b^{(1)}(\omega) = (\epsilon_i(\omega)/\epsilon_0 - 1)$  is the bulk linear susceptibility of the metal,  $e$  is the electron charge (absolute value),  $n_0$  is the number density of the conduction electrons,  $\omega_p$  is the plasma frequency and  $\epsilon_0$  is the permittivity of the vacuum. By choosing  $a = 1$ ,  $b = -1$  and  $d = 1$  we obtain the Rudnick-Stern hydrodynamic model [33, 34]. The mesh has a number of edges equal to  $N_e = 3747$ . The maximum expansion order of vector spherical wave functions, used in the calculation of the SH-Mie solution, is  $N = 10$ . Aiming at an accurate validation of the proposed approach, we show in fig. 2 the quantity  $dP^{(2\omega)}/d\Omega$  as a function of the inclination angle  $\theta$  for  $\phi = 0$  and  $\phi = 90$ . These quantities have been calculated by the SH-Mie (orange triangles for  $\phi = 0$  and red circles for  $\phi = 90$ ) and by the SH-SIE (continuous black line for  $\phi = 0$  and continuous blue line for  $\phi = 90$ ). Several sphere's diameters  $D$  have been considered: the first row of fig. 2 (panels a-d), is relative to an electrically small particle with  $D = 20nm$ , the second row (e-h) to  $D = 100nm$ , the third row (i-l) to  $D = 200nm$ . We considered in the first three columns only one SH source at a time, whereas in the fourth column the different nonlinear polarization sources are simultaneously active. In particular, in the first column of fig. 2, corresponding to panels (a,e,i), we considered only the nonlocal-bulk source  $P_n^{\gamma'}$  using the coefficients  $(\gamma, \chi_{\parallel\perp\parallel}^{(2)}, \chi_{\perp\perp\perp}^{(2)}) = (1, 0, 0)$ . In the second column (b,f,j) only the surface source  $P_t^S$  has been considered assuming  $(\gamma, \chi_{\parallel\perp\parallel}^{(2)}, \chi_{\perp\perp\perp}^{(2)}) = (0, 1, 0)$ , whereas in the third column (c,g,k) only the surface source  $P_n^S$  has been considered assuming  $(\gamma, \chi_{\parallel\perp\parallel}^{(2)}, \chi_{\perp\perp\perp}^{(2)}) = (0, 0, 1)$ . Eventually, in panels (d,h,l,p) we considered a realistic physical case in which the different weights are calculated using eq. 34 with  $(a, b, d) = (1, -1, 1)$ . In all the different cases shown in fig. 2 very good agreement between the SH-SIE and the SH-Mie formulations can be found.

In Fig. 3 we calculate the relative error  $\xi$  of the SH-SIE formulation with respect to the SH-Mie formulation, defined as:

$$\xi = \left( dP^{(2\omega)}/d\Omega - P_{\text{MIE}}^{(2\omega)}/d\Omega \right) / \left( P^{(2\omega)}/d\Omega \right), \quad (35)$$

where  $P_{\text{MIE}}^{(2\omega)}/d\Omega$  is the radiated power per unit solid angle calculate with the SH-Mie formulation. The error is plotted as a function of inclination angle  $\theta$  for (a)  $\phi = 0$  and (b)  $\phi = 90$  for of the for the  $D = 100nm$  sphere. All the investigated cases present a comparable error, below 3%. Only in correspondence of the forward and backward scattering direction, when the corresponding value of  $dP^{(2\omega)}/d\Omega$  is very small the error is higher.

In figure 4 we show the radiation diagram of  $dP^{(2\omega)}/d\Omega$  for different diameters of the sphere,  $D =$  (a)  $20nm$  (b)  $100nm$  (c)  $200nm$ . The SH radiated power vanishes for the forward and backscattering directions for all the investigated diameters, because the sphere is rotationally symmetric around the propagation direction. As we in-

crease the sphere's diameter we notice the appearance of multiple oscillations corresponding to high order modes. Moreover, as the particle size increases, the inclination angle corresponding to the first maximum SH intensity approaches the forward scattering direction. This behavior has been experimentally demonstrated for silver spherical particles in a recent work by Gonella *et al.* [35].

We now consider a triangular nano-prism of height  $h = 40nm$  with rounded edges of length  $200nm$ . The radius of the osculating cylinder (sphere) at each edge (corner) is  $10nm$ . This shape is of extreme interest in nanoplasmonics as the building block of bow-tie nano-antennas, whose SH properties have been recently investigated in [36]. We chose as the exciting wavelength  $\lambda = 690nm$ , corresponding to the peak of the extinction cross section over the visible range. Due to the irregular shape the distribution of the field will be highly inhomogeneous and the relaxation term of the free-electron in the hydrodynamic model has to be considered [14, 15, 37, 38]. As a consequence, we correct the Rudnick-Stern coefficients following ref. [14]. Moreover, the contribution due to  $\delta'$  is non-vanishing; it is related to  $\gamma$  by [14, 15, 38]:

$$\delta' = -\frac{2}{1 + j\omega\tau}\gamma$$

where  $\tau = 9.3 \cdot 10^{-15}$  [31]. We first analyze the scattering properties at the fundamental frequency. In figure 5 (a,c) we show the magnitude of the total electric field at the fundamental frequency on the surface of the triangular nano-prism when the incident plane wave is polarized along (a) the  $x$  axis and (c) the  $y$  axis. When the incident plane wave is x-polarized two *hot spots* arise at the two ends of the edge parallel to the incident polarization, whereas in correspondence of a y-polarized excitation the remaining corner experiences the highest field enhancement. The radiated power  $dP^{(\omega)}/d\Omega$  at the fundamental frequency can be attributed to an electric dipole oriented along the polarization direction (inset of Fig. 5 (a,c)). In panels (b,d) we study the SH radiated power  $dP^{(2\omega)}/d\Omega$  by the triangular nano-prism. Unlike the linear scattering,  $dP^{(2\omega)}/d\Omega$  shows a richer behavior dominated by higher order modes. Furthermore, the shape of  $dP^{(2\omega)}/d\Omega$  is affected by the distribution of the electric field on the surface of the particle, shown in fig. 5 (a,b). In fact, we attribute the presence of the two lobes in panel to the strong field localization that occurs in correspondence of the two corners of the edge of the triangular-nanoprism parallel to x-axis. In contrast, when the incident field is directed along the y-axis, the radiation diagram features one lobe driven by the hot-spot on the remaining corner. Although both the surface area and the volume of the nano-prisms are lower than those of the sphere of diameter  $200nm$  investigated earlier, the maximum intensity of SH radiated power per unit solid angle  $dP^{(2\omega)}/d\Omega$  of the nano-prism (Fig. 5(b,d)) is almost two order of magnitude higher compared to the sphere (Fig. 4 (b)). This fact is due to both the higher values of the non-linear susceptibilities of gold at  $690nm$

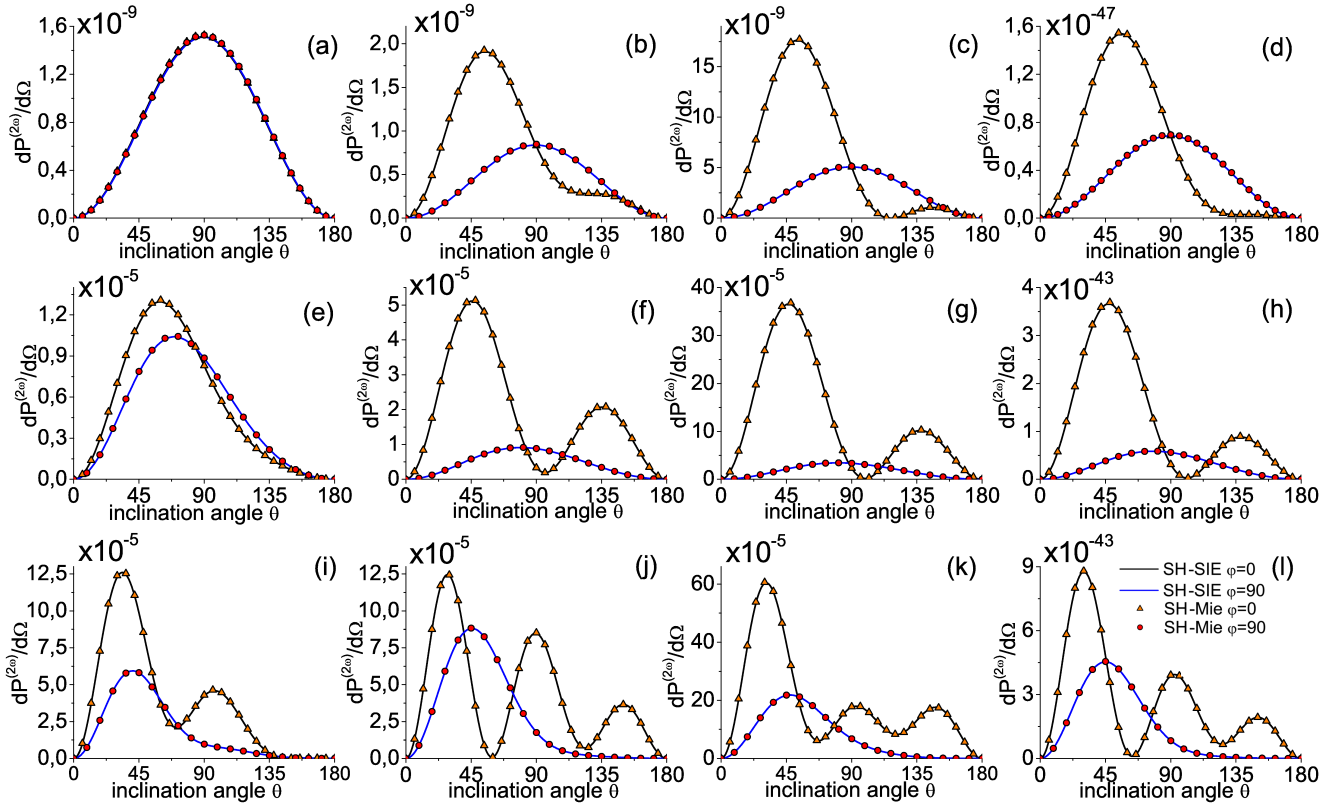


FIG. 2. SH radiated power per unit solid angle (expressed in Watt/Steradian) of a gold sphere with diameter (a-d) 20nm, (e-h) 100nm (i-l) 200nm. Different combinations of SHG polarization sources have been considered, namely  $(\gamma, \chi_{\parallel\perp\parallel}^{(2)}, \chi_{\perp\perp\perp}^{(2)}) = (1, 0, 0)$  in panels (a,e,i);  $(0, 1, 0)$  in panels (b,f,j);  $(0, 0, 1)$  in panels (c,g,k). In panels (d,h,l) the sources have been weighted using eq. 34 with  $(a, b, d) = (1, -1, 1)$ . The sphere is excited by a x-polarized plane wave of unitary intensity propagating along the positive  $z$  axis with wavelength 520nm. The diagrams are in linear scale.

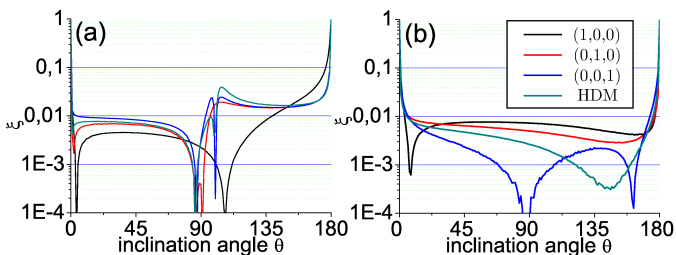


FIG. 3. Relative error of  $dP^{(2\omega)}/d\Omega$  calculated with the SH-SIE with respect to the SH-Mie solution for a sphere of diameter  $D = 100\text{nm}$  as a function of the inclination angle  $\theta$  for (a)  $\phi = 0$  and (b)  $\phi = 90$ . Different combinations of SHG polarization sources have been considered, namely  $(\gamma, \chi_{\parallel\perp\parallel}^{(2)}, \chi_{\perp\perp\perp}^{(2)}) = (1, 0, 0)$  (black line);  $(0, 1, 0)$  (red line);  $(0, 0, 1)$  (blue line); the hydrodynamic model of eq. 34 with  $(a, b, d) = (1, -1, 1)$  (green line).

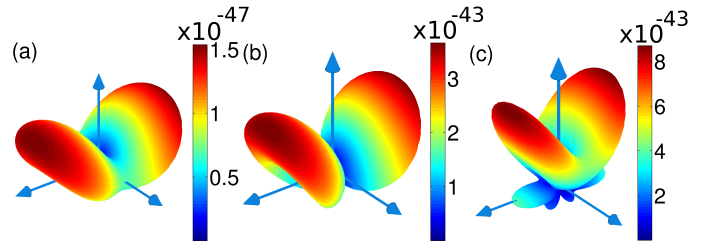


FIG. 4. Radiation diagram of  $dP^{(2\omega)}/d\Omega$  (expressed in Watt/Steradian) for a gold sphere with diameter: (a) 20nm, (b) 100nm (c) 200nm. The sphere is excited by a x-polarized plane wave of unitary intensity propagating along the positive direction of the  $z$ -axis with wavelength 520nm. The radiated power is evaluated at 260nm. The diagrams are in linear scale. The sources have been weighted using eq. 34 with  $(a, b, d) = (1, -1, 1)$ .

## VI. CONCLUSIONS

We have presented a surface integral equation method to solve the second harmonic generation problem in centrosymmetric nanoparticles with arbitrary shapes and to the NP asymmetric shape [39].



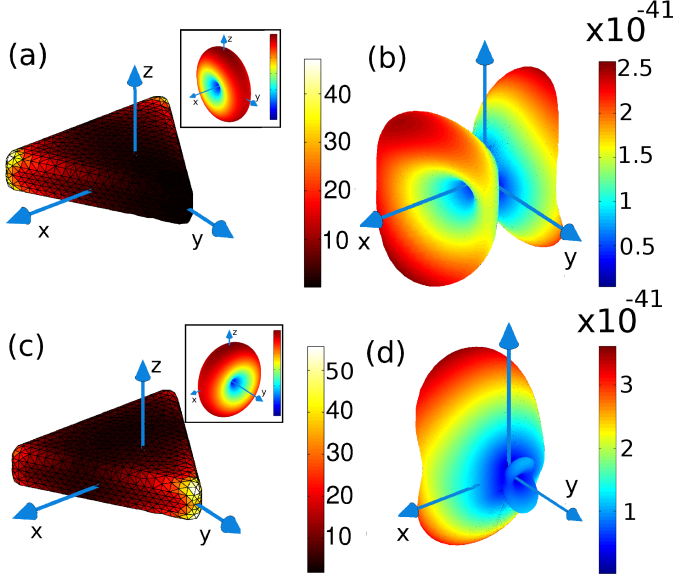


FIG. 5. (a,c) Magnitude of the field  $\mathbf{E}_e^{(\omega)}$  at the fundamental frequency on the surface of the triangular nano-prism excited by a monochromatic ( $\lambda = 690\text{nm}$ ) plane wave of unitary intensity propagating along the positive  $z$ -axis and linearly polarized along (a)  $x$  and (c)  $y$ , and the corresponding radiated power per unit solid angle (inset). (b,d) Radiation diagram of  $dP^{(2\omega)}/d\Omega$  (expressed in Watt/Steradian) for both the (b)  $x$ -polarized and (d)  $y$ -polarized pump.

counting for both the nonlocal-bulk and local-surface nonlinear polarization sources. We have demonstrated that the contribution of the nonlocal-bulk nonlinear polarization sources to the SH electromagnetic field can be taken into account by introducing equivalent elec-

tric and magnetic currents on the nanoparticle boundary. We compared our numerical solution to the analytical Mie solution for spheres of several radii, obtaining very good agreement for any investigated case. The developed method paves the way to a better understanding of the process of SHG in arbitrarily shaped nanoparticles. This approach can have a high impact in the design of novel nanoplasmonic devices with enhanced SHG emission, including for instance sensor probing physical and chemical properties of material surfaces.

## VII. ACKNOWLEDGEMENT

This work was partly supported by the Italian Ministry of Education, University and Research through the project PON01\_02782.

### Appendix A: Electromagnetic field generated by surface sources

In the present section, we provide the expression of the electromagnetic field generated by a surface distribution of electric and magnetic currents ( $\mathbf{j}^{(\Omega,e)}, \mathbf{j}^{(\Omega,m)}$ ) defined on  $S$  and radiating in a homogeneous medium with constitutive parameters ( $\epsilon_l\{\Omega\}, \mu_l$ ) at frequency  $\Omega$ . The electromagnetic field radiated by both the electric and magnetic currents is [40]:

$$\mathbf{E}^{(\Omega)}(\mathbf{r}) = \mathcal{E}_l^{(\Omega)} \left\{ \mathbf{j}^{(\Omega,e)}, \mathbf{j}^{(\Omega,m)} \right\}(\mathbf{r}) \quad (\text{A1a})$$

$$\mathbf{H}^{(\Omega)}(\mathbf{r}) = \mathcal{H}_l^{(\Omega)} \left\{ \mathbf{j}^{(\Omega,e)}, \mathbf{j}^{(\Omega,m)} \right\}(\mathbf{r}) \quad (\text{A1b})$$

where:

$$\begin{aligned} \mathcal{E}_l^{(\Omega)} \left\{ \mathbf{j}^{(\Omega,e)}, \mathbf{j}^{(\Omega,m)} \right\} &= \zeta_l \{\Omega\} \mathcal{T}_l^{(\Omega)} \left\{ \mathbf{j}^{(\Omega,e)} \right\} + \mathcal{K}_l^{(\Omega)} \left\{ \mathbf{j}^{(\Omega,m)} \right\} + \begin{cases} \mathbf{0} & \text{if } \mathbf{r} \notin S, \\ +\frac{\zeta_l \{\Omega\}}{2jk_l \{\Omega\}} [\nabla_S \cdot \mathbf{j}^{(\Omega,e)}] \mathbf{n} - \frac{1}{2} \mathbf{n} \times \mathbf{j}^{(\Omega,m)} & \text{if } \mathbf{r} \in S_i, \\ -\frac{\zeta_l \{\Omega\}}{2jk_l \{\Omega\}} [\nabla_S \cdot \mathbf{j}^{(\Omega,e)}] \mathbf{n} + \frac{1}{2} \mathbf{n} \times \mathbf{j}^{(\Omega,m)} & \text{if } \mathbf{r} \in S_e, \end{cases} \\ \mathcal{H}_l^{(\Omega)} \left\{ \mathbf{j}^{(\Omega,e)}, \mathbf{j}^{(\Omega,m)} \right\} &= -\mathcal{K}_l^{(\Omega)} \left\{ \mathbf{j}^{(\Omega,e)} \right\} + \frac{\mathcal{T}_l^{(\Omega)} \left\{ \mathbf{j}^{(\Omega,m)} \right\}}{\zeta_l \{\Omega\}} + \begin{cases} \mathbf{0} & \text{if } \mathbf{r} \notin S, \\ +\frac{1}{2} \mathbf{n} \times \mathbf{j}^{(\Omega,e)}(\mathbf{r}) + \frac{[\nabla_S \cdot \mathbf{j}^{(\Omega,m)}(\mathbf{r})]}{2j\zeta_l \{\Omega\} k_l \{\Omega\}} \mathbf{n} & \text{if } \mathbf{r} \in S_i, \\ -\frac{1}{2} \mathbf{n} \times \mathbf{j}^{(\Omega,e)}(\mathbf{r}) - \frac{[\nabla_S \cdot \mathbf{j}^{(\Omega,m)}(\mathbf{r})]}{2j\zeta_l \{\Omega\} k_l \{\Omega\}} \mathbf{n} & \text{if } \mathbf{r} \in S_e, \end{cases} \end{aligned} \quad (\text{A2})$$

$\nabla_S \cdot$  denotes the surface divergence,  $\mathcal{K}_l$  and  $\mathcal{T}_l$  denote the integral operators:

$$\mathcal{K}_l^{(\Omega)} \{ \mathbf{w} \}(\mathbf{r}) = - \int_S \mathbf{w}(\mathbf{r}') \times \nabla' g_l^{(\Omega)}(\mathbf{r} - \mathbf{r}') dS' \quad (\text{A3a})$$

$$\begin{aligned} \mathcal{T}_l^{(\Omega)} \{ \mathbf{w} \}(\mathbf{r}) &= -jk_l \{\Omega\} \int_S g_l^{(\Omega)}(\mathbf{r} - \mathbf{r}') \mathbf{w}(\mathbf{r}') dS' + \\ &- \frac{1}{jk_l \{\Omega\}} \int_S \nabla' g_l^{(\Omega)}(\mathbf{r} - \mathbf{r}') \nabla'_S \cdot \mathbf{w}(\mathbf{r}') dS' \end{aligned} \quad (\text{A3b})$$

$g_l^{(\Omega)}$  is the homogeneous space Green's function, *i.e.*  $g_l^{(\Omega)}(\mathbf{r} - \mathbf{r}') = \frac{e^{-jk_l \{\Omega\} |\mathbf{r} - \mathbf{r}'|}}{4\pi |\mathbf{r} - \mathbf{r}'|}$ ,  $k_l \{\Omega\} = \Omega \sqrt{\mu_l \epsilon_l \{\Omega\}}$ .

$$\mathcal{K}_l^{(\Omega,t)} \{ \cdot \} = -\mathbf{n} \times \mathbf{n} \times \mathcal{K}_l^{(\Omega)} \{ \cdot \} \Big|_{S_i} \quad (\text{A4a})$$

$$\mathcal{T}_l^{(\Omega,t)} \{ \cdot \} = -\mathbf{n} \times \mathbf{n} \times \mathcal{T}_l^{(\Omega)} \{ \cdot \} \Big|_{S_i}. \quad (\text{A4b})$$

## Appendix B: Excitation Vectors

Now we calculate the discrete excitation vector associated to the superficial vector field  $\boldsymbol{\pi}_m^{(2\omega)}$ :

$$\langle \mathbf{f}_p, \boldsymbol{\pi}_S^{(m)} \rangle = \iint_{\Sigma} \mathbf{f}_p \cdot \boldsymbol{\pi}_S^{(m)} dS \quad (\text{B1})$$

Using eqs. 7b and 31 we obtain:

$$\begin{aligned} \langle \mathbf{f}_p, \boldsymbol{\pi}_S^{(m)} \rangle = & \\ & \frac{1}{\varepsilon_0} \sum_{j=2,3,4} \iint_{\Sigma} \left( P_n^S|_{T_j} - P_n^S|_{T_1} \right) \mathbf{f}_p \cdot \mathbf{n} \times \mathbf{m}_{j1} \delta_{j1} dS \\ & + \frac{1}{\varepsilon_0} \sum_{j=5,6} \iint_{\Sigma} \left( P_n^S|_{T_j} - P_n^S|_{T_2} \right) \mathbf{f}_p \cdot \mathbf{n} \times \mathbf{m}_{j2} \delta_{j2} dS \end{aligned} \quad (\text{B2})$$

It is worth noting that the function  $\mathbf{f}_p$  and  $\mathbf{n}$  is discontinuous in  $\Sigma$ . Therefore, we have to use the following properties of the Dirac delta function. Let  $\mathbf{F}$  be a function defined as  $\mathbf{F}(\mathbf{r}) = \mathbf{F}|_{T_1}(\mathbf{r})$  if  $\mathbf{r} \in T_j$  where each function  $\mathbf{F}|_{T_1}$  is regular in the interior of the triangle  $T_j$ . The following relation holds in the distribution sense:

$$\mathbf{F} \delta_{l_{j1}} = \frac{\mathbf{F}|_{T_j} + \mathbf{F}|_{T_1}}{2} \delta_{l_{j1}} \quad (\text{B3})$$

Applying this property to the integrands of eq. B2 and exploiting the fact that  $\mathbf{f}_p = 0$  in  $T_3, T_4, T_5, T_6$ ,  $\mathbf{f}_p = \mathbf{f}_p^+$  in  $T_1$  and  $\mathbf{f}_p = \mathbf{f}_p^-$  in  $T_2$  we obtain:

$$\begin{aligned} \mathbf{f}_p \cdot \mathbf{n} \times \mathbf{m}_{j1} \delta_{j1} = & \\ & \begin{cases} \frac{1}{2} \mathbf{f}_p^+ \cdot \mathbf{n}_1 \times \mathbf{m}_{j1} \delta_{j1} & j=3,4 \\ \frac{1}{2} (\mathbf{f}_p^+ \cdot \mathbf{n}_1 \times \mathbf{m}_{j1} + \mathbf{f}_p^- \cdot \mathbf{n}_2 \times \mathbf{m}_{j1}) \delta_{j1} & j=2 \end{cases} \end{aligned}$$

$$\mathbf{f}_p \cdot \mathbf{n} \times \mathbf{m}_{j2} \delta_{j2} = (\mathbf{f}_p^- \cdot \mathbf{n}_2 \times \mathbf{m}_{j2}) \delta_{j2} \quad j=5,6$$

Therefore, using the sampling property of the Dirac delta function eq. B2 becomes:

$$\begin{aligned} \langle \mathbf{f}_p, \boldsymbol{\pi}_m^{(S)} \rangle = & \frac{1}{2\varepsilon_0} \sum_{j=2,3,4} \left( P_n^S|_{T_j} - P_n^S|_{T_1} \right) \int_{l_{j1}} \mathbf{f}_p^+ \cdot \mathbf{t}_{j1} dl \\ & + \frac{1}{2\varepsilon_0} \sum_{j=1,5,6} \left( P_n^S|_{T_j} - P_n^S|_{T_2} \right) \int_{l_{j2}} \mathbf{f}_p^- \cdot \mathbf{t}_{j2} dl \end{aligned}$$

Moreover, since we have  $\oint_{\partial T_1} \mathbf{f}_p^+ \cdot d\mathbf{l} = 0$  and  $\oint_{\partial T_2} \mathbf{f}_p^- \cdot d\mathbf{l} = 0$  we finally obtain:

$$\begin{aligned} \langle \mathbf{f}_p, \boldsymbol{\pi}_m^{(S)} \rangle = & \frac{1}{2\varepsilon_0} \sum_{j=2,3,4} P_n^S|_{T_j} \int_{l_{j1}} \mathbf{f}_p^+ \cdot \mathbf{t}_{j1} dl \\ & + \frac{1}{2\varepsilon_0} \sum_{j=1,5,6} P_n^S|_{T_j} \int_{l_{j2}} \mathbf{f}_p^- \cdot \mathbf{t}_{j2} dl \end{aligned}$$

In conclusion, in order to compute the term  $\langle \mathbf{f}_p, \boldsymbol{\pi}_S^{(m)} \rangle$  we have to consider not only the value of  $P_n^S$  in the triangles  $T_p^+$  and  $T_p^-$  but also in the 4 adjacent triangles that have one edge in common with  $T_p^+$  and  $T_p^-$ .

Using a similar derivation and exploiting the fact that  $\mathbf{f}_p^+ \cdot \mathbf{n}_1 \times \mathbf{n}_1 \times \mathbf{m}_{j1} = \mathbf{0}$  with  $j = 3, 4$  and  $\mathbf{f}_p^- \cdot \mathbf{n}_2 \times \mathbf{n}_2 \times \mathbf{m}_{j2} = \mathbf{0}$  with  $j = 5, 6$  it is possible to prove that:

$$\begin{aligned} \langle \mathbf{f}_p, \mathbf{n} \times \boldsymbol{\pi}_S^{(m)} \rangle = & \\ & - \frac{1}{2\varepsilon_0} \left( P_n^S|_{T_1} - P_n^S|_{T_2} \right) \mathbf{m}_{12} \cdot \int_{l_{12}} (\mathbf{f}_p^+ + \mathbf{f}_p^-) dl = \\ & \frac{l_p}{\varepsilon_0} \left( P_n^S|_{T_1} - P_n^S|_{T_2} \right) \end{aligned}$$

The treatment of the excitation terms arising from the bulk source  $P_n^{\gamma'}$  follows the same steps of  $P_n^S$

$$\begin{aligned} \langle \mathbf{f}_p, \boldsymbol{\pi}_{\gamma'}^{(m)} \rangle = & \\ & \frac{1}{2\varepsilon_0} \sum_{j=2,3,4} \int_{l_{j1}} \left( P_n^{\gamma'}|_{T_j} + P_n^{\gamma'}|_{T_1} \right) \mathbf{f}_p^+ \cdot \mathbf{t}_{j1} dl \\ & + \frac{1}{2\varepsilon_0} \sum_{j=1,5,6} \int_{l_{j2}} \left( P_n^{\gamma'}|_{T_j} + P_n^{\gamma'}|_{T_2} \right) \mathbf{f}_p^- \cdot \mathbf{t}_{j2} dl \end{aligned}$$

Using similar arguments it is possible to demonstrate that:

$$\begin{aligned} \langle \mathbf{f}_p, \mathbf{n} \times \boldsymbol{\pi}_{\gamma'}^{(m)} \rangle = & \\ & \frac{1}{\varepsilon_0} \iint_{T_1} \nabla_S \cdot \mathbf{f}_p^+ P_n^{\gamma'}|_{T_1} dS + \frac{1}{\varepsilon_0} \iint_{T_2} \nabla_S \cdot \mathbf{f}_p^- P_n^{\gamma'}|_{T_2} dS \end{aligned}$$

In order to evaluate the excitation terms relative to  $\mathbf{P}_{\delta'}$  we have to perform volumetric integrals and therefore we introduce a tetrahedral mesh of the particle volume  $V_i$ . The derivation of the corresponding source terms is straightforward in the Galerkin formalism. Using eqs. 17 and 11 we have:

$$\begin{aligned} \langle \mathbf{f}_p, \boldsymbol{\pi}_{\delta'}^{(m)} \rangle = & \sum_{r=\pm} \left\{ \right. \\ & - j\omega\mu_0 \iint_{T_p^r} \mathbf{n} \times \mathbf{f}_p(\mathbf{r}) \cdot \left[ \iiint_{V_i} \mathbf{J}_{\delta}(\mathbf{r}') g_i(\mathbf{r} - \mathbf{r}') dV' \right] dS \\ & + \frac{1}{\varepsilon_i \{2\omega\}} \iiint_{V_i} \rho_{\delta}(\mathbf{r}') \left[ \oint_{\partial T_p^r} g_i(\mathbf{r} - \mathbf{r}') \mathbf{f}_p(\mathbf{r}) \cdot d\mathbf{l} \right] dV' \\ & \left. + \frac{1}{\varepsilon_i \{2\omega\}} \iint_{T_p^r} \eta_{\delta}(\mathbf{r}') \left[ \oint_{\partial T_p^r} g_i(\mathbf{r} - \mathbf{r}') \mathbf{f}_p(\mathbf{r}) \cdot d\mathbf{l} \right] dS' \right\} \end{aligned}$$

$$\begin{aligned}
\langle \mathbf{f}_p, \mathbf{n} \times \boldsymbol{\pi}_{\delta'}^{(m)} \rangle &= \sum_{r=\pm} \left\{ \right. \\
&- j\omega\mu_0 \iint_{T_p^r} \mathbf{f}_p(\mathbf{r}) \cdot \left[ \iiint_{V_i} \mathbf{J}_\delta(\mathbf{r}) g_i(\mathbf{r}-\mathbf{r}') dV' \right] dS \\
&+ \frac{1}{\varepsilon_i \{2\omega\}} \iint_{V_i} \rho_\delta(\mathbf{r}') \left[ \iint_{T_p^r} g_i(\mathbf{r}-\mathbf{r}') \nabla_S \cdot \mathbf{f}_p(\mathbf{r}) dS \right] dV' \\
&+ \left. \frac{1}{\varepsilon_i \{2\omega\}} \iint_{T_p^r} \eta_\delta(\mathbf{r}') \left[ \iint_{T_p^r} g_i(\mathbf{r}-\mathbf{r}') \nabla_S \cdot \mathbf{f}_p(\mathbf{r}) dS \right] dS' \right\}
\end{aligned}$$

Using eqs. 17 and 12 we have:

$$\begin{aligned}
\langle \mathbf{f}_p, \mathbf{n} \times \boldsymbol{\pi}_{\delta'}^{(e)} \rangle &= \\
&- \sum_{r=\pm} \iint_{V_i} \mathbf{J}_\delta(\mathbf{r}') \cdot \iint_{T_p^r} (\mathbf{n} \times \mathbf{f}_p) \times \nabla g(\mathbf{r}-\mathbf{r}') dS dV' \\
\langle \mathbf{f}_p, \boldsymbol{\pi}_{\delta'}^{(e)} \rangle &= \\
&- \sum_{r=\pm} \iint_{V_i} \mathbf{J}_\delta(\mathbf{r}') \cdot \iint_{T_p^r} \mathbf{f}_p \times \nabla g(\mathbf{r}-\mathbf{r}') dS dV'
\end{aligned}$$

- 
- [1] M. Kauranen and A. V. Zayats, “Nonlinear plasmonics,” *Nature Photonics*, vol. 6, pp. 737–748.
- [2] Maier, *Plasmonics: Fundamental and Applications*. Springer, 2007.
- [3] A. Bouhelier, M. Beversluis, A. Hartschuh, and L. Novotny, “Near-field second-harmonic generation induced by local field enhancement,” *Phys. Rev. Lett.*, vol. 90, p. 013903, Jan 2003.
- [4] T. F. Heinz, “Chapter 5,” in *Nonlinear Surface Electromagnetic Phenomena* (H.-E. Ponath and G. I. Stegeman, eds.), pp. 397–405, North-Holland, Amsterdam, 1991.
- [5] J. I. Dadap, J. Shan, K. B. Eisenthal, and T. F. Heinz, “Second-harmonic rayleigh scattering from a sphere of centrosymmetric material,” *Phys. Rev. Lett.*, vol. 83, pp. 4045–4048, Nov 1999.
- [6] Guyot-Sionnest, W. Chen, and Y. R. Shen, “General considerations on optical second-harmonic generation from surfaces and interfaces,”
- [7] W. L. Mochán, J. A. Maytorena, B. S. Mendoza, and V. L. Brudny, “Second-harmonic generation in arrays of spherical particles,” *Phys. Rev. B*, vol. 68, p. 085318, Aug 2003.
- [8] J. I. Dadap, J. Shan, and T. F. Heinz, “Theory of optical second-harmonic generation from a sphere of centrosymmetric material: small-particle limit,” *J. Opt. Soc. Am. B*, vol. 21, pp. 1328–1347, Jul 2004.
- [9] Y. Pavlyukh and W. Hübner, “Nonlinear mie scattering from spherical particles,” *Phys. Rev. B*, vol. 70, p. 245434, Dec 2004.
- [10] J. Xu and X. Zhang, “Second harmonic generation in three-dimensional structures based on homogeneous centrosymmetric metallic spheres,” *Opt. Express*, vol. 20, pp. 1668–1684, Jan 2012.
- [11] C. I. Valencia, E. R. Méndez, and B. S. Mendoza, “Second-harmonic generation in the scattering of light by an infinite cylinder,” *J. Opt. Soc. Am. B*, vol. 21, pp. 36–44, Jan 2004.
- [12] A. G. F. de Beer, S. Roke, and J. I. Dadap, “Theory of optical second-harmonic and sum-frequency scattering from arbitrarily shaped particles,” *J. Opt. Soc. Am. B*, vol. 28, pp. 1374–1384, Jun 2011.
- [13] J. Mäkitalo, S. Suuriniemi, and M. Kauranen, “Boundary element method for surface nonlinear optics of nanoparticles,” *Opt. Express*, vol. 19, pp. 23386–23399, Nov 2011.
- [14] A. Benedetti, M. Centini, M. Bertolotti, and C. Sibilia, “Second harmonic generation from 3d nanoantennas: on the surface and bulk contributions by far-field pattern analysis,” *Opt. Express*, vol. 19, pp. 26752–26767, Dec 2011.
- [15] F. X. Wang, F. J. Rodriguez, W. M. Albers, R. Ahorinta, J. E. Sipe, and M. Kauranen, “Surface and bulk contributions to the second-order nonlinear optical response of a gold film,” *Phys. Rev. B*, vol. 80, p. 233402, Dec 2009.
- [16] A. Capretti, C. Forestiere, L. Dal Negro, and G. Miano, “Second harmonic generation in spherical metallic nanoparticles: a full wave analysis with both local surface and nonlocal bulk polarization sources,” *Submitted to Phys. Rev. B*, 2012.
- [17] R. Harrington, *Time-Harmonic Electromagnetic Fields*. Springer, 2007.
- [18] P. M. Taskinen, Ylä-Oijala, and S. Järvenpää, “Surface integral equation formulations for solving electromagnetic scattering problems with iterative methods,” *Radio Sci.*, vol. 40, oct. 2005.
- [19] L. N. Medgyesi-Mitschang, J. M. Putnam, and M. B. Gedera, “Generalized method of moments for three-dimensional penetrable scatterers,” *J. Opt. Soc. Am. A*, vol. 11, pp. 1383–1398, Apr 1994.
- [20] J. Aizpurua, P. Hanarp, D. S. Sutherland, M. Käll, G. W. Bryant, and F. J. Garcia de Abajo, “Optical properties of gold nanorings,” *Phys. Rev. Lett.*, vol. 90, p. 057401, Feb 2003.
- [21] G. W. Bryant, F. J. Garcia de Abajo, and J. Aizpurua, “Mapping the plasmon resonances of metallic nanoantennas,” *Nano Letters*, vol. 8, no. 2, pp. 631–636, 2008. PMID: 18189444.
- [22] A. M. Kern and O. J. F. Martin, “Surface integral formulation for 3d simulations of plasmonic and high permittivity nanostructures,” *J. Opt. Soc. Am. A*, vol. 26, pp. 732–740, Apr 2009.
- [23] B. Gallinet, A. M. Kern, and O. J. F. Martin, “Accurate and versatile modeling of electromagnetic scattering on periodic nanostructures with a surface integral approach,” *J. Opt. Soc. Am. A*, vol. 27, pp. 2261–2271, Oct 2010.
- [24] J. M. Taboada, J. Rivero, F. Obelleiro, M. G. Araújo, and L. Landesa, “Method-of-moments formulation for the analysis of plasmonic nano-optical antennas,” *J. Opt. Soc. Am. A*, vol. 28, pp. 1341–1348, Jul 2011.
- [25] C. Forestiere, A. J. Pasquale, A. Capretti, G. Miano, A. Tamburrino, S. Y. Lee, B. M. Reinhard, and L. Dal Negro, “Genetically engineered plasmonic nanoarrays,”

- Nano Letters*, vol. 12, no. 4, pp. 2037–2044, 2012.
- [26] N. Bloembergen, R. K. Chang, S. S. Jha, and C. H. Lee, “Optical second-harmonic generation in reflection from media with inversion symmetry,” *Phys. Rev.*, vol. 174, pp. 813–822, Oct 1968.
- [27] J. E. Sipe, V. Mizrahi, and G. I. Stegeman, “Fundamental difficulty in the use of second-harmonic generation as a strictly surface probe,” *Phys. Rev. B*, vol. 35, pp. 9091–9094, Jun 1987.
- [28] R. Harrington, *Field Computation by Moment Methods*. New York: Macmillan, 1968.
- [29] S. Rao, D. Wilton, and A. Glisson, “Electromagnetic scattering by surfaces of arbitrary shape,” *Antennas and Propagation, IEEE Transactions on*, vol. 30, pp. 409–418, may 1982.
- [30] R. Graglia, “On the numerical integration of the linear shape functions times the 3-d green’s function or its gradient on a plane triangle,” *Antennas and Propagation, IEEE Transactions on*, vol. 41, pp. 1448–1455, oct 1993.
- [31] P. B. Johnson and R. W. Christy, “Optical constants of the noble metals,” *Phys. Rev. B*, vol. 6, pp. 4370–4379, Dec 1972.
- [32] G. Bachelier, J. Butet, I. Russier-Antoine, C. Jonin, E. Benichou, and P.-F. Brevet, “Origin of optical second-harmonic generation in spherical gold nanoparticles: Local surface and nonlocal bulk contributions,” *Phys. Rev. B*, vol. 82, p. 235403, Dec 2010.
- [33] J. E. Sipe, V. C. Y. So, M. Fukui, and G. I. Stegeman, “Analysis of second-harmonic generation at metal surfaces,” *Phys. Rev. B*, vol. 21, pp. 4389–4402, May 1980.
- [34] J. Rudnick and E. A. Stern, “Second-harmonic radiation from metal surfaces,” *Phys. Rev. B*, vol. 4, pp. 4274–4290, Dec 1971.
- [35] G. Gonella, W. Gan, B. Xu, and H.-L. Dai, “The effect of composition, morphology, and susceptibility on nonlinear light scattering from metallic and dielectric nanoparticles,” *The Journal of Physical Chemistry Letters*, vol. 3, no. 19, pp. 2877–2881, 2012.
- [36] T. Hanke, G. Krauss, D. Träutlein, B. Wild, R. Bratschitsch, and A. Leitenstorfer, “Efficient nonlinear light emission of single gold optical antennas driven by few-cycle near-infrared pulses,” *Phys. Rev. Lett.*, vol. 103, p. 257404, Dec 2009.
- [37] A. Benedetti, M. Centini, C. Sabilia, and M. Bertolotti, “Engineering the second harmonic generation pattern from coupled gold nanowires,” *J. Opt. Soc. Am. B*, vol. 27, pp. 408–416, Mar 2010.
- [38] M. Centini, A. Benedetti, M. Scalora, C. Sabilia, and M. Bertolotti, “Second harmonic generation from metallic 2d scatterers,” pp. 73540F–73540F–9, 2009.
- [39] B. K. Canfield, H. Husu, J. Laukkanen, B. Bai, M. Kuitinen, J. Turunen, and M. Kauranen, “Local field asymmetry drives second-harmonic generation in noncentrosymmetric nanodimers,” *Nano Letters*, vol. 7, no. 5, pp. 1251–1255, 2007.
- [40] J. G. Van Bladel, *Electromagnetic Fields*. IEEE Press Series on Electromagnetic Wave Theory, 2007.